Journal of Biomolecular NMR
https://doi.org/10.1007/s10858-019-00240-w

ARTICLE

Detection of chemical exchange in methyl groups of macromolecules

Michelle L. Gill[1,2] · Andrew Hsu[3] · Arthur G. Palmer[1]

Received: 9 October 2018 / Accepted: 8 March 2019

Abstract
The zero- and double-quantum methyl TROSY Hahn-echo and the methyl ^{1}H–^{1}H dipole–dipole cross-correlation nuclear magnetic resonance experiments enable estimation of multiple quantum chemical exchange broadening in methyl groups in proteins. The two relaxation rate constants are established to be linearly dependent using molecular dynamics simulations and empirical analysis of experimental data. This relationship allows chemical exchange broadening to be recognized as an increase in the Hahn-echo relaxation rate constant. The approach is illustrated by analyzing relaxation data collected at three temperatures for *E. coli* ribonuclease HI and by analyzing relaxation data collected for different cofactor and substrate complexes of *E. coli* AlkB.

Keywords AlkB · Cross-correlated relaxation · Double-quantum relaxation · Dynamics · Multiple-quantum relaxation · Ribonuclease HI · Zero-quantum relaxation

Introduction

An important first step in characterizing micro-to-millisecond time scale dynamic processes in proteins and other biological macromolecules consists of identifying which sites are subject to significant chemical exchange broadening in NMR spectroscopic experiments (Palmer and Koss 2019). A very general approach relies on the scaling of chemical exchange broadening with the magnitude of the static magnetic field (Phan et al. 1996; O'Connell et al. 2009; Millet and Palmer 2000). Other approaches rely on high-power spin-locking radiofrequency fields to suppress chemical exchange broadening for comparison with a reference experiment in which exchange is minimally suppressed (Ban et al. 2013; Reddy et al. 2018; Hansen et al. 2009). For backbone ^{15}N spins in {U-^{2}H, U-^{15}N} proteins, the TROSY Hahn-echo experiment is very efficient (Wang and Palmer 2003). In this experiment, the exchange-free relaxation rate constant is estimated as $R_2^0 = \kappa\eta_{xy}$ in which η_{xy} is the transverse ^{1}H–^{15}N dipole/^{15}N CSA transverse relaxation interference rate constant, which depends on physical parameters and can be calculated a priori, or more often measured empirically, for a subset of spins not subject to exchange (Kroenke et al. 1998; Fushman and Cowburn 1998).

Relaxation of ^{1}H and ^{13}C spins in methyl groups is a powerful probe of side-chain conformational dynamics, and experimental methods for measurement of single- and multiple-quantum relaxation rate constants have been developed extensively by Kay and coworkers (Tugarinov et al. 2003, 2004, 2005, 2006, 2007; Korzhnev et al. 2004a, b; Tugarinov and Kay 2006, 2007). We described zero- and double-quantum methyl TROSY Hahn-echo experiments (Gill and Palmer 2011) and subsequently used these experiments in an investigation of the role of conformational dynamics in gating activity of the *E. coli* DNA repair enzyme AlkB (Ergel et al. 2014). The Hahn-echo experiment minimally suppresses chemical exchange effects; consequently, exchange can be detected by comparison with a second experiment that either suppresses chemical exchange (Toyama et al. 2016) or that is independent of chemical exchange (Toyama et al. 2017). Herein, the methyl ^{1}H–^{1}H dipole–dipole cross-correlation experiment developed by Tugarinov et al. (2007) serves as the exchange-free reference experiment. The combination of methyl TROSY Hahn-echo and methyl ^{1}H–^{1}H dipole–dipole cross-correlation experiments allows

✉ Arthur G. Palmer
agp6@columbia.edu

[1] Department of Biochemistry and Molecular Biophysics, Columbia University, 630 West 168th Street, New York, NY 10032, USA

[2] BenevolentAI, 81 Prospect St, Brooklyn, NY 11201, USA

[3] Department of Chemistry, Columbia University, 3000 Broadway, New York, NY 10027, USA

Published online: 12 August 2019

facile identification of chemical exchange in methyl groups (Toyama et al. 2017). The approach is illustrated for both *E. coli* ribonuclease HI (RNase H) and AlkB.

The expression for differential relaxation of zero- and double-quantum coherence (ΔR_{MQ}) measured in the Hahn-echo experiments is:

$$\Delta R_{MQ} = (R_{DQ} - R_{ZQ})/2 = \Delta R^0 + \Delta R_{ex}/2 \tag{1}$$

in which (Tugarinov et al. 2004; Gill and Palmer 2011; Konrat and Sterk 1993; Norwood et al. 1999):

$$\Delta R^0 = \frac{2}{5}\left(\frac{\mu_0}{4\pi}\right)^2 \hbar\tau_c\gamma_c\gamma_H^3 \left\{ \frac{8\gamma_D^2}{3\gamma_H^2} \sum_{D^E} \left\langle \frac{P_2(\cos\theta_{CD^EH})}{(r_{CD^E} r_{HD^E})^3} \right\rangle + \sum_{H^E} \left\langle \frac{P_2(\cos\theta_{CH^EH})}{(r_{CH^E} r_{HH^E})^3} \right\rangle \right\} = \frac{2}{5}\left(\frac{\mu_0}{4\pi}\right)^2 \hbar^2\tau_c\gamma_c\gamma_H^3\Gamma \tag{2}$$

$$\Delta R_{ex} = 4p_1p_2\Delta\omega_C\Delta\omega_H/k_{ex} \tag{3}$$

μ_0 is the vacuum permeability, $\hbar$ is Planck's constant divided by 2π, τ_c is the effective overall rotational correlation time of the macromolecule, γ_X is the magnetogyric ratio (X = C, D, and H to represent ^{13}C, ^{2}H, and ^{1}H, respectively), r_{CD^E} and r_{HD^E} are the distances from the methyl ^{13}C and ^{1}H to remote ^{2}H spins in the molecule, r_{CH^E} and r_{HH^E} are the distances from the methyl ^{13}C and ^{1}H to remote ^{1}H spins in the protein, $P_2(x) = (3x^2 - 1)/2$ is the second Legendre polynomial, and θ_{CXH} is the angle between the C–X–H atoms. The term in brackets has been denoted Γ for convenience. The first summation is over all the remote ^{2}H spins and the second summation is over all the remote ^{1}H spins in the molecule; the relative size of these two summations depends upon the pattern and extent of deuteration of the protein and the fractional content of D_2O in the sample buffer (vide infra). Angle brackets indicate ensemble averaging to account for fast molecular dynamics. Rotation of the methyl group was treated by averaging distances for the three methyl H-atom positions. The expression for ΔR_{ex} is the fast-limit expression for two-site exchange for convenience; in this expression, p_1 and p_2 are the populations of the two states of the molecule, $\Delta\omega_C$ and $\Delta\omega_H$ are the differences in ^{13}C and ^{1}H chemical shifts for a spin in the two states, $k_{ex} = k_1 + k_{-1}$, and k_1 and k_{-1} are the forward and reverse reaction rate constants. Expressions for ΔR_{ex} for other time scales have been given in the literature (Wang and Palmer 2002). The ^{1}H–^{1}H dipole–dipole cross-correlated relaxation rate constant for pairs of ^{1}H spins in a methyl group is given by (Tugarinov et al. 2007):

$$\eta_{HH} = \frac{9}{10}\left(\frac{\mu_0}{4\pi}\right)^2 \hbar^2\gamma_H^4 P_2(\cos\theta_{HH})^2 S_{axis}^2 \tau_c \left\langle r_{HH}^{-6} \right\rangle \tag{4}$$

in which $\theta_{HH} = \pi/2$ is the angle between a vector of length r_{HH} between two ^{1}H spins in the methyl group and the methyl symmetry axis, and S_{axis}^2 is the generalized order parameter for a unit vector along the symmetry axis of the methyl group. Importantly, this rate constant is independent of any exchange contributions.

Experimental data reported below for RNase H suggest a linear correlation exists between ΔR^0 and η_{HH} and hence between Γ and S_{axis}^2:

$$\Gamma = \alpha S_{axis}^2 + \beta \tag{5}$$

This correlation also is supported by molecular dynamics (MD) simulations (vide infra) and reflects the dependence of both Γ and S_{axis}^2 on packing density (Trott et al. 2008; Zhang and Brüschweiler 2002; Ming and Brüschweiler 2004). Combining Eqs. 2, 4, and 5 yields:

$$\Delta R^0 = \frac{4}{9}P_2(\cos\theta_{HH})^{-2}\left\langle r_{HH}^{-6}\right\rangle\gamma_c\gamma_H^{-1}\alpha\eta_{HH} + \frac{2}{5}\left(\frac{\mu_0}{4\pi}\right)^2\hbar^2\tau_c\gamma_c\gamma_H^3\beta = \kappa\eta_{HH} + \varepsilon \tag{6}$$

The values of α and β, or κ and ε, can be estimated from MD simulations, or by examining the distribution of experimental values of ΔR_{MQ} relative to η_{HH}, because contributions from ΔR_{ex} will only increase ΔR_{MQ}. Combining Eqs. 1 and 6 yields $\Delta R_{ex} = 2(\Delta R_{MQ} - \eta_{HH} - \varepsilon)$ as the key result for detection of chemical exchange contributions to multiple quantum relaxation in methyl spin systems.

Methods

Molecular dynamics simulations

A full description of the MD simulations and comparison with NMR spin relaxation data for RNase H will be published elsewhere. Briefly, the system was prepared and simulations were performed using the Schrödinger Maestro Protein Preparation Wizard version 11.3.016 (Banks et al. 2005; Sastry et al. 2013), Schrödinger Multisim version 3.8.5.19 (Banks et al. 2005), and Desmond version 5.5 (Sastry et al. 2013). Hydrogen atoms were added to the X-ray crystal structure (PDB code 2RN2, 1.5 Å resolution) consistent with pH = 5.5 to mimic the conditions used in NMR experiments; solvated with TIP3P water in an orthorhombic box with a 10 Å buffer region from solute to box boundary (Jorgensen et al. 1983); and neutralized with Cl^- ions. The system was relaxed and energy-minimized prior to a 5 ns constant pressure and constant temperature (NPT) equilibration simulation. Twenty structures were extracted from the trajectory (structures were chosen roughly every 250 ps with the proviso that the box volume was close to the average box volume over the 5 ns of the simulation). These structures were ranked based on their MolProbity score (Chen et al. 2010; Williams et al. 2018) and the top two structures were chosen

as the starting structures for two independent 1-μs constant volume and constant temperature (NVT) simulations. Volume and temperature reached equilibrium values in less than 100 ps in all simulations. A RESPA integrator was used with a time step of 1 fs for bonded and short-range non-bonded interactions, and 3 fs for long-range electrostatics (Tuckerman et al. 1992). Electrostatics were calculated with the particle mesh Ewald method using a 9 Å cutoff (Cheatham et al. 1995; Darden et al. 1993; York et al. 1993). Simulations were performed at 300 K using a Nosé-Hoover thermostat (Nosé 1984; Hoover 1985). Additionally, the NPT ensemble used a Martyna–Tobias–Klein (MTK) barostat (Martyna et al. 1994). Coordinate sets were saved every 10 ps for NPT simulations and 4.5 ps for NVT simulations.

NMR spectroscopy

$^{13}C^{\varepsilon}$-methionine AlkB was expressed and purified and the NMR spin relaxation parameters were determined at 21.1 T as previously described (Ergel et al. 2014). The expression and purification of U-^{2}H and [^{13}C $^{1}H_3$] Ile δ1 and stereospecifically labeled Val γ and Leu δ RNase H has also been described (Gill and Palmer 2011). For RNase H, all NMR experiments were performed on a Bruker Avance spectrometer with a triple resonance z-axis gradient cryoprobe and operating at 14.1 T. Each experiment was performed at 283, 300, and 310 K, and the Hahn echo data collected at 283 K have been previously reported (Gill and Palmer 2011). Temperature was calibrated using 98% $^{2}H_4$-methanol (Findeisen et al. 2007). The zero- and double-quantum Hahn echo data collected at 300 and 310 K used 1024 × 188 ($t_2 \times t_1$) complex points, 4.5 × 7.2 kHz spectral widths, and relaxation delays of $n/(2J_{CH})$ where $J_{CH} = 128$ Hz and $n = \{1, 25, 40\}$ for 300 K and $n = \{1, 10, 25, 35, 40, 45\}$ for 310 K. The ^{1}H–^{1}H cross correlated relaxation data were collected with 1024 × 256 complex points, 4.9 × 7.3 kHz spectral widths, and relaxation delays of 2, 8, 20, 40, and 50 ms at each of the three temperatures. Data were processed with NMRPipe (Delaglio et al. 1995) using a cosine bell function for apodization in the indirect dimension. Assignments were made using Sparky (2008). Peak intensities for the Hahn Echo data acquired at 283 K were determined from ten iterative rounds of peak fitting performed in NMRPipe, as described previously (Gill and Palmer 2011). The remaining peak intensities were determined using Sparky. Further data analysis and visualization of results were performed using Python (Helmus and Jaroniec 2013; McKinney 2010; Millman and Aivazis 2011; Oliphant 2007; Pérez et al. 2007; van der Walt et al. 2011; Hunter and Matplotlib 2007).

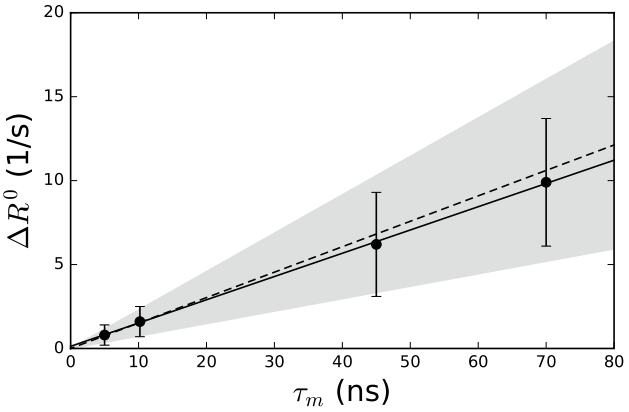

Fig. 2 Experimental and predicted values of ΔR^0 versus τ_c. Solid, circles: Experimental values of ΔR_{MQ} measured for protein L (5 and 25 °C) and malate synthase G (20 and 37 °C), assuming minimal contributions from exchange (Tugarinov et al. 2004). Dashed: Average values calculated from the values of Γ determined from MD simulations of RNase H. The shaded region shows ± 1 standard deviation of the calculations. Calculations were performed for the 25 methyl groups used in Fig. 1

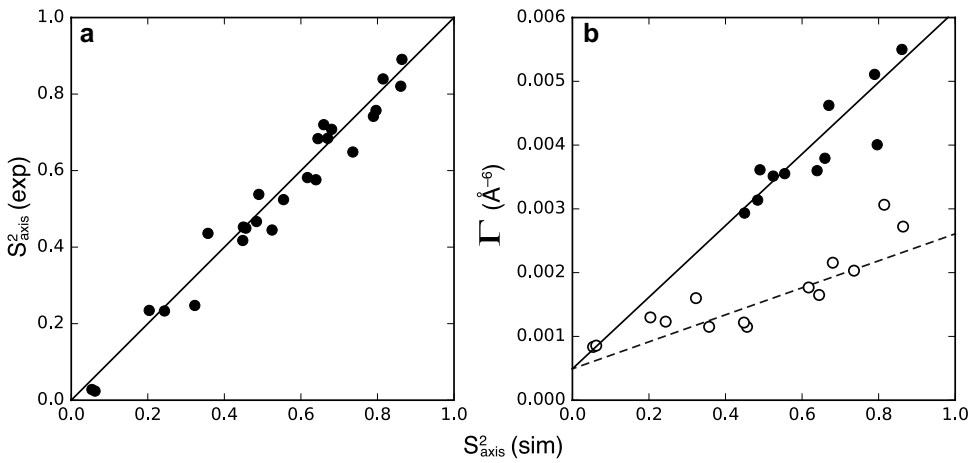

Fig. 1 **a** Comparison between experimental and MD simulated values of S^2_{axis} for 25 methyl groups for which the absolute deviation is < 0.1. **b** Values of Γ determined from MD simulations are plotted versus the simulated values of S^2_{axis} for the same methyl groups shown in (**a**). Two lines are plotted for the (solid symbols, solid line) subset of data with maximum slope and (empty symbols, dashed line) subset of data with minimum slope. The intercepts of the plotted lines are set equal to the fitted line for dashed line

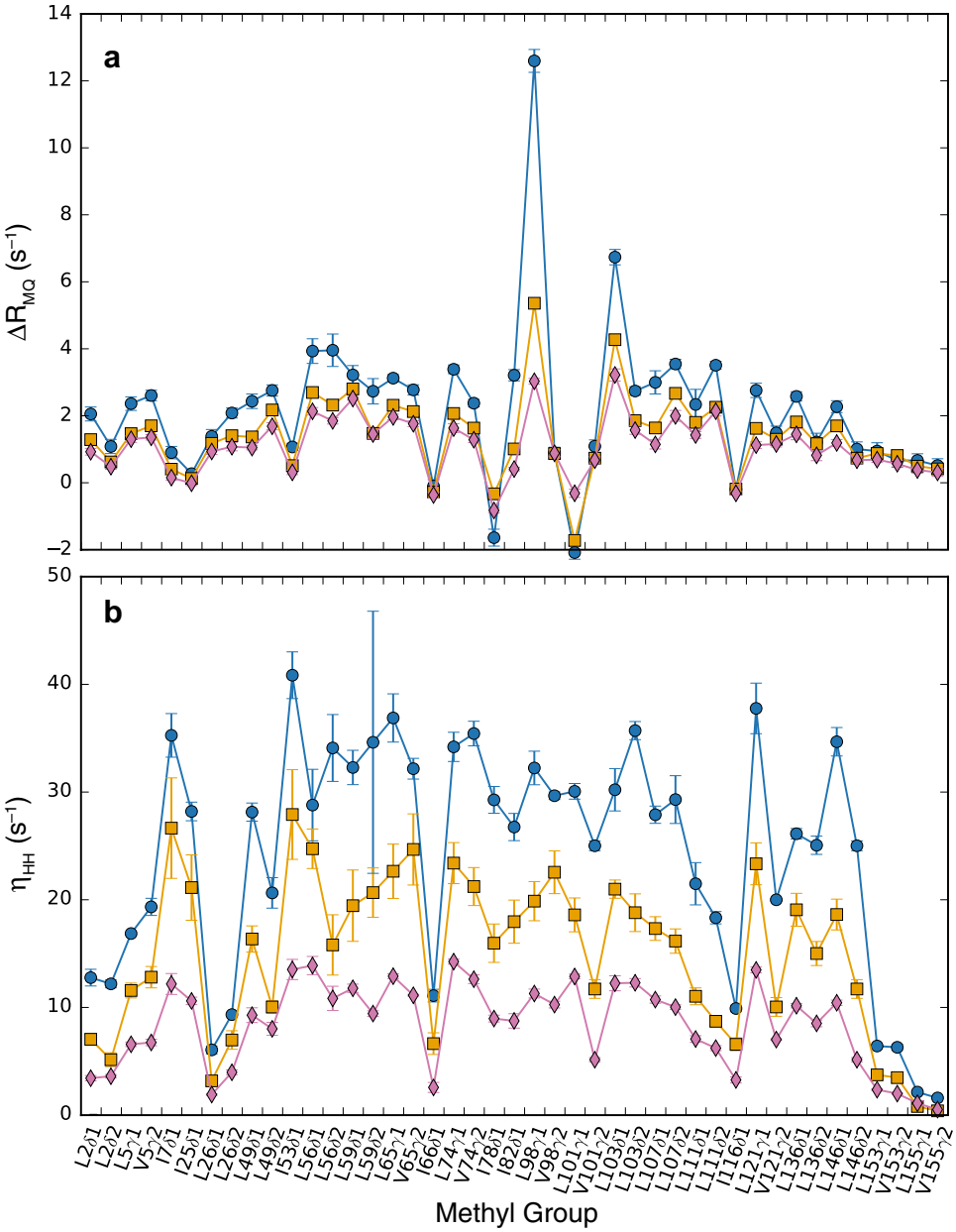

Fig. 3 **a** Differential relaxation rate of zero- and double-quantum coherence (ΔR_{MQ}) and **b** ^{1}H–^{1}H dipole–dipole cross-correlated relaxation rate constant (η_{HH}) for Ile, Leu, and Val residues of RNase H measured at (blue, circles) 283, (orange, squares) 300, and (reddish-purple, diamonds) 310 K, respectively

Results and discussion

The bracketed term denoted Γ in Eq. 2 must be calculated from MD simulations or estimated empirically. In the present work, this term was calculated for Ile γ1, Leu γ1 and γ2, and Val γ1 and γ2 methyl groups in RNase H as the average value from two 1-μs MD simulations. The calculations included the 25 (out of 46) methyl groups for which the absolute differences between simulated and experimental values of S^2_{axis} were less than 0.1; however, results were not substantially altered by changing the maximum difference to 0.05 or 0.15. The experimental values of S^2_{axis} are described elsewhere (Hsu et al. 2018) and compared to simulated values in Fig. 1a. The graph of Γ versus the simulated value of S^2_{axis} is shown in Fig. 1b. The calculated points cluster into two subsets with different slopes. The slopes were determined using the non-parametric Thiel-Sen estimator. The intercepts for both sets of data were set to the intercept determined for the subset of data with the smaller slope. The fitted values of α gave low and high estimates of $\kappa_{ILV} = 0.030$ and 0.080, respectively. The fitted value of β gave $\varepsilon_{ILV} = 0.37\ s^{-1}$.

The calculations were validated by calculating ΔR^0 from Eq. 1 for the same 25 methyl groups used for Fig. 1 and comparing to the mean values of ΔR_{MQ} for protein L and malate synthase G reported by Kay and coworkers (Tugarinov et al.

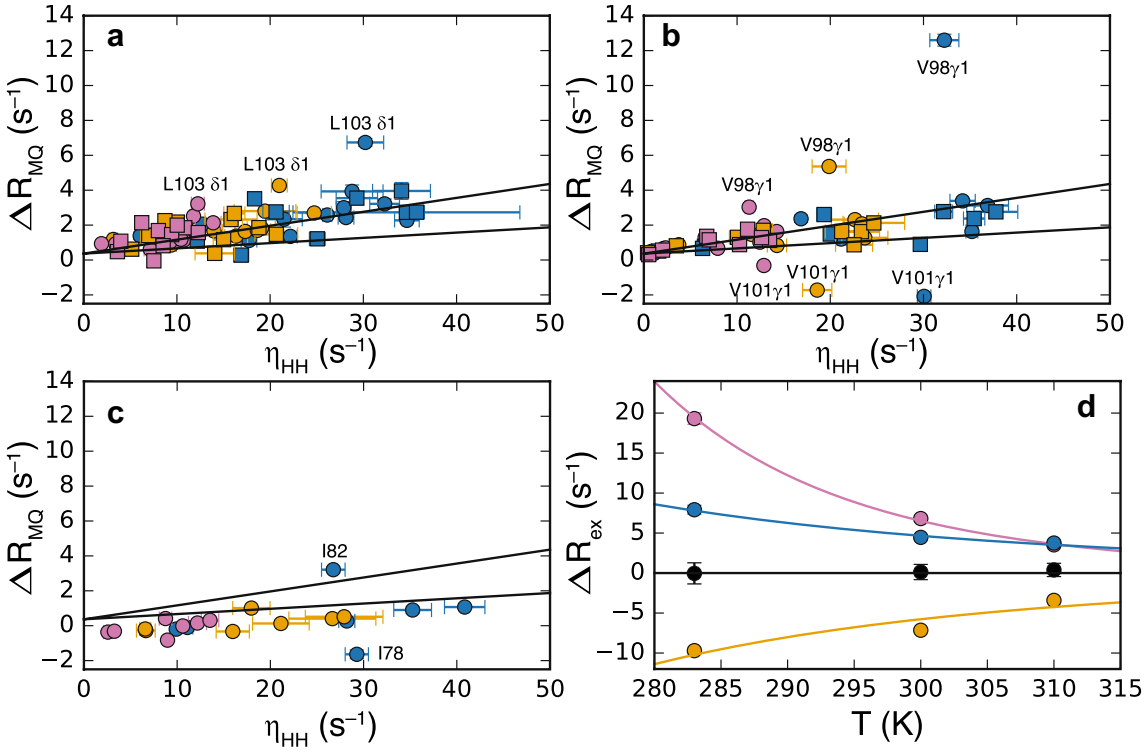

Fig. 4 Values of ΔR_{MQ} versus η_{HH} are shown for RNase H **a** Leu γ1 (circles) and γ2 (squares), **b** Val γ1 (circles) and γ2 (squares), and **c** Ile γ1 methyl groups at (blue) 283 K, (orange) 300 K, and (reddish-purple) 310 K. The solid line is the mean result calculated as $\kappa_{ILV}\,\eta_{HH}$. The shaded region shows ± 1 standard deviation in the mean of the calculation. **d** Arrhenius plot for (reddish-purple) Val 98 γ1, (orange) Val 101 γ1, (blue) Leu 103 γ1, and (black, circles) mean of all other Leu and Val residues. Solid lines for Val 98 γ1, Val 101 γ1, and Leu 103 γ1 show best single-exponential fits to the data to obtain $E^{\dagger}_{app}$, given in Table 1

Table 1 Apparent activation energies

Residue	Activation energy ($E^{\dagger}_{app}$, kJ/mol)
Val 98 γ1	45.4 ± 1.6
Val 101 γ1	23.7 ± 1.9
Leu103 δ1	21.4 ± 3.0

Estimated apparent activation energies ($E^{\dagger}_{app}$) as determined from the temperature dependence of ΔR_{ex} versus 1/T using Eq. 6, as shown in Fig. 4d

2004). A graph of the experimental and predicted results is shown in Fig. 2. The predicted slope differs from the fitted slope by ~ 10%, well within the spread of experimental values, and the standard deviation of the predicted slope is in good agreement with the experimental standard deviations shown in the figure. For the highly deuterated RNase H sample, the predicted relaxation contribution from remote ^{2}H spins (the first sum in Eq. 2) is ~ 10-fold larger than from remote ^{1}H spins (the second sum in Eq. 2).

The values of ΔR_{MQ} and η_{HH} for Ile γ1, Leu γ1 and γ2, and Val γ1 and γ2 methyl groups in RNase H at 283, 300, and 310 K are shown in Fig. 3. Graphs of ΔR_{MQ} versus η_{HH} are shown in Fig. 4. Lines plotted using the calculated values of κ_{ILV} and ε_{ILV} are shown. The differences between the lines shown for the two estimates of κ_{ILV} set a lower bound on the smallest exchange contribution that can be detected by this method. Note that ΔR_{ex}, and hence ΔR_{MQ}, can be negative depending on the relative signs of $\Delta\omega_C$ and $\Delta\omega_H$, as shown by Eq. 3. Larger values of $|\Delta R_{MQ}|$ for Val 98 γ1, Val 101 γ1, and Leu 103 γ1 are consistent with significant conformational exchange; elevated values of $|\Delta R_{MQ}|$ also are observed for Ile 78 γ1 and Ile 82 γ1 at 283 K. Excluding these residues, a linear fit to ΔR_{MQ} versus η_{HH} using the 'leiv' Bayesian algorithm in the statistics program R gave $\kappa_{ILV} = 0.094 \pm 0.003$ and $\varepsilon_{ILV} = 0.01 \pm 0.03$, in good agreement with the larger of the two values of κ_{ILV} obtained from the MD simulations.

The resonances of Val 98 γ1, Val 101 γ1, and Leu 103 γ1 are notably broadened, beyond that of the other residues in RNase H. Graphs of ΔR_{ex} versus $1/T$ for these residues are shown in Fig. 4d. For fast-limit two-site exchange with site populations $p_1 \gg p_2$, the apparent activation energy is (Butterwick et al. 2004):

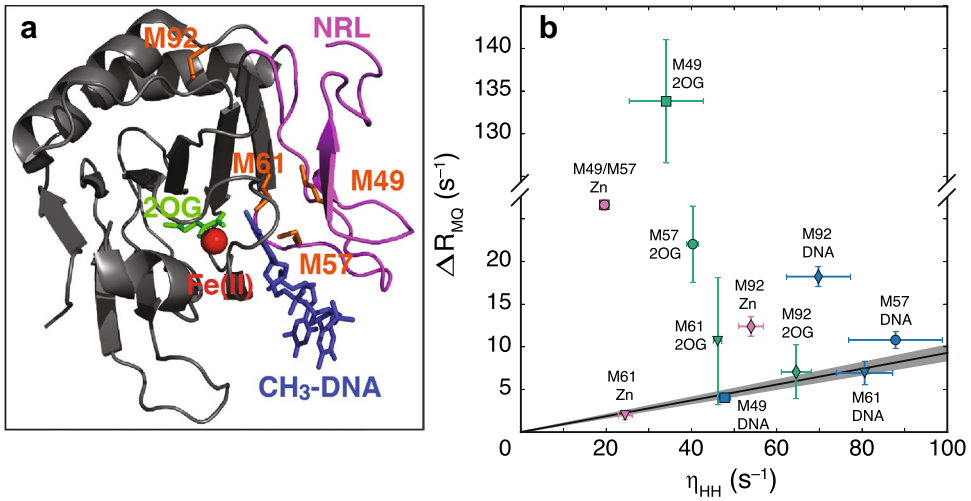

Fig. 5 Chemical exchange in AlkB. **a** Ribbon diagram showing the crystal structure of AlkB-N11 with bound Fe(II) (red), 2-oxoglutarate (2OG, green), and methylated DNA substrate (blue) drawn from PDB code 2FD8. The Fe(II)/2OG core and nucleotide recognition lid are colored grey and magenta, respectively, and the residues used as spectroscopic probes are shown in orange stick representation. **b** Values of ΔR_{MQ} versus η_{HH} are shown for AlkB. M49 (squares), M57 (circles), M61 (triangles) and M92 (diamonds) are shown for AlkB in successive complex with Zn^{2+} (reddish-purple), Zn^{2+}/2OG (green), and Zn^{2+}/2OG/DNA substrate (blue). The solid line is the mean empirical result calculated as $\kappa_{Met}\eta_{HH}$ (see main text). The shaded region shows ± the standard deviation of the calculations. M49 and M57 are degenerate in the Zn^{2+} complex

$$E^{\dagger}_{app} = E^{\dagger}_{1} + \Delta E(1 - 3p^{0}_{1}) = \bar{E}^{\dagger} - \Delta E(p^{0}_{1} - p^{0}_{2}) \quad (7)$$

in which $E^{\dagger}_{1}$, and $E^{\dagger}_{-1}$ are the activation barriers in the forward and reverse reaction directions, $\Delta E = E^{\dagger}_{1} - E^{\dagger}_{-1}$, p^{0}_{1} and p^{0}_{2} are the site populations at a reference temperature T^{0}, and $\bar{E}^{\dagger} = p^{0}_{2}E^{\dagger}_{1} + p^{0}_{1}E^{\dagger}_{-1}$ is the apparent activation energy that would be obtained from $d\ln(k_{ex})/d(1/T)$ rather than $d\ln(\Delta R_{ex})/d(1/T)$. Consequently, $E^{\dagger}_{app}$ underestimates $\bar{E}^{\dagger}$ by $\Delta E(p^{0}_{1} - p^{0}_{2}) \approx \Delta E$. Values of $E^{\dagger}_{app}$ are given in Table 1 for Val 98 γ1, Val 101 γ1, and Leu103 γ1. Values of the activation barriers are consistent with results from $R_{1\rho}$ measurements for backbone ^{15}N spins (Butterwick and Palmer 2006). Each of these residues has been demonstrated to be directly involved in or located within the substrate-binding handle region associated with conformational transitions from open to closed states by ^{15}N amide spin relaxation experiments and/or molecular dynamics simulations (Butterwick and Palmer 2006; Stafford et al. 2013, 2015).

Figure 5 shows a graph of ΔR_{MQ} versus η_{HH} based on data previously reported (see Fig. 5c, d in Ergel et al. (2014)) for the DNA repair enzyme AlkB in complex with Zn^{2+}; Zn^{2+} and the co-substrate 2-oxoglutarate (2OG); and Zn^{2+}, 2OG, and DNA substrate 5′-CAmAAT-3′. Results are shown for the four Met residues in AlkB: Met 49, Met 57, and Met 61 are located in the active site or nucleotide recognition lid (NRL) and Met 92 is located at a hinge between the core domain and the NRL. A number of residues in the various complexes exhibit conformational exchange broadening, with the largest ΔR_{ex} observed for M49 in the 2OG complex. Notably, the NMR spectra of the methyl groups of Met 49, Met 57 and Met 61 in the ternary complex show sharp resonance signals (Ergel et al. 2014), suggesting that exchange is absent for the active site residues in this complex. As shown above for RNase H, ε has a small effect on the analysis; accordingly, ε_{Met} was set to zero and the weighted-mean ratio $\Delta R_{MQ}/\eta_{HH} = 0.093 \pm 0.009$ for Met 49, Met 57 and Met 61 was set to κ_{Met}. These results are consistent with exchange between an open and closed conformer in the Zn and Zn/2OG enzyme complexes, and with significant line broadening of M49 in the 2OG complex due to nearly equal populations of open and closed conformations in the Zn/2OG complex and a relatively large chemical shift difference between the two states ($\Delta\omega_C >= 2.1$ ppm) for this residue (Ergel et al. 2014; Bleijlevens et al. 2008, 2012).

Conclusion

The combination of the zero- and double-quantum methyl TROSY Hahn-echo experiment (Gill and Palmer 2011) and the methyl ^{1}H–^{1}H dipole–dipole cross-correlation experiment (Tugarinov et al. 2007) provide a convenient experimental approach to determining $\Delta R_{ex} = 2(\Delta R_{MQ} - \kappa\eta_{HH} - \varepsilon)$ in a fashion that is analogous to the ^{1}H–^{15}N TROSY Hahn-echo experiment. The proportionality constant κ can be calculated accurately from MD simulations

or from empirical comparisons between ΔR_{MQ} and η_{HH} and depends on the labeling strategy employed; the intercept ε is small in the examples considered herein. Application of this approach to relaxation data collected at three temperatures identifies residues Val 98, Val 101, and Leu 103 as key probes of conformational dynamics of the substrate binding handle region of RNase H. A second application of this approach confirms previous observations that chemical exchange broadening reflects an open-closed equilibrium of nucleotide recognition lid of AlkB. These applications suggest that the proposed approach has wide application in studies of the conformational dynamics of proteins and other biological macromolecules (Toyama et al. 2017).

Acknowledgements Support from National Institutes of Health grants GM089047 (M.L.G.), GM008281 (A. H.). and GM050291 (A.G.P.) is acknowledged gratefully. The AVANCE 600 NMR spectrometer at Columbia University was purchased with the support of NIH grant RR026540. Some of the work presented here was conducted at the Center on Macromolecular Dynamics by NMR Spectroscopy located at the New York Structural Biology Center, supported by a grant from the NIH National Institute of General Medical Sciences (P41 GM118302). A.G.P. is a member of the New York Structural Biology Center. A preliminary account of this work was presented as poster 96 at the 56th Experimental NMR Conference (2016). We thank Richard Friesner (Columbia University) and Martha Beckwith (Advanced Science Research Center, City University of New York) for helpful discussions and Richard Friesner for access to computational facilities. This paper is dedicated to Dennis Torchia (National Institutes of Health) on occasion of his 80th birthday in appreciation of his pioneering achievements in NMR spectroscopy, spin relaxation, and protein dynamics.

References

Ban D, Mazur A, Carneiro MG, Sabo TM, Giller K, Koharudin LM, Becker S, Gronenborn AM, Griesinger C, Lee D (2013) Enhanced accuracy of kinetic information from CT-CPMG experiments by transverse rotating-frame spectroscopy. J Biomol NMR 57:73–82

Banks JL, Beard HS, Cao Y, Cho AE, Damm W, Farid R, Felts AK, Halgren TA, Mainz DT, Maple JR, Murphy R, Philipp DM, Repasky MP, Zhang LY, Berne BJ, Friesner RA, Gallicchio E, Levy RM (2005) Integrated Modeling Program, Applied Chemical Theory (IMPACT). J Comput Chem 26:1752–1780

Bleijlevens B, Shivarattan T, Flashman E, Yang Y, Simpson PJ, Koivisto P, Sedgwick B, Schofield CJ, Matthews SJ (2008) Dynamic states of the DNA repair enzyme AlkB regulate product release. EMBO Rep 9:872–877

Bleijlevens B, Shivarattan T, van den Boom KS, de Haan A, van der Zwan G, Simpson PJ, Matthews SJ (2012) Changes in protein dynamics of the DNA repair dioxygenase AlkB upon binding of Fe^{2+} and 2-oxoglutarate. Biochemistry 51:3334–3341

Butterwick JA, Palmer AG (2006) An inserted gly residue fine tunes dynamics between mesophilic and thermophilic ribonucleases H. Protein Sci 15:2697–2707

Butterwick JA, Loria P, Astrof J, Kroenke NS, Cole CD, Rance R, M. & Palmer AG (2004) Multiple time scale backbone dynamics of homologous thermophilic and mesophilic ribonuclease HI enzymes. J Mol Biol 339:855–871

Cheatham TE III, Miller JL, Fox T, Darden TA, Kollman PA (1995) Molecular dynamics simulations on solvated biomolecular systems: The particle mesh Ewald method leads to stable trajectories of DNA, RNA, and proteins. J Am Chem Soc 117:4193–4194

Chen VB, Arendall WB 3rd, Headd JJ, Keedy DA, Immormino RM, Kapral GJ, Murray LW, Richardson JS, Richardson DC (2010) MolProbity: all-atom structure validation for macromolecular crystallography. Acta Crystallogr D Biol Crystallogr 66:12–21

Darden T, York D, Pedersen L (1993) Particle mesh Ewald: an N·log(N) method for Ewald sums in large systems. J Chem Phys 98:10089–10092

Delaglio F, Grzesiek S, Vuister GW, Zhu G, Pfeifer J, Bax A (1995) NMRPipe: a multidimensional spectral processing system based on UNIX pipes. J Biomol NMR 6:277–293

Ergel B, Gill ML, Brown L, Yu B, Palmer AG, Hunt JF (2014) Protein dynamics control the progression and efficiency of the catalytic reaction cycle of the *Escherichia coli* DNA-repair enzyme AlkB. J Biol Chem 289:29584–29601

Findeisen M, Brand T, Berger S (2007) A ^{1}H–NMR thermometer suitable for cryoprobes. Magn Reson Chem 45:175–178

Fushman D, Cowburn D (1998) Model-independent analysis of ^{15}N chemical shift anisotropy from NMR relaxation data. Ubiquitin as a test example. J Am Chem Soc 120:7109–7110

Gill ML, Palmer AG (2011) Multiplet-filtered and gradient-selected zero-quantum TROSY experiments for $^{13}C^{1}H_3$ methyl groups in proteins. J Biomol NMR 51:245–251

Goddard T, Kneller DG (2008) SPARKY 3. University of California, San Francisco

Hansen DF, Feng H, Zhou Z, Bai Y, Kay LE (2009) Selective characterization of microsecond motions in proteins by NMR relaxation. J Am Chem Soc 131:16257–16265

Helmus JJ, Jaroniec CP (2013) NMRglue: an open source Python package for the analysis of multidimensional NMR data. J Biomol NMR 55:355–367

Hoover WG (1985) Canonical dynamics: equilibrium phase-space distributions. Phys Rev A 31:1695–1697

Hsu A, O' Brien PA, Bhattacharya S, Rance M, Palmer AG (2018) Enhanced spectral density mapping through combined multiple-field deuterium $^{13}CH_2D$ methyl spin relaxation NMR spectroscopy. Methods 139:76–84

Hunter JD, Matplotlib (2007) A 2D graphics environment. IEEE Comput Sci Eng 9:90–95

Jorgensen WL, Chandrasekhar J, Madura JD, Impey RW, Klein ML (1983) Comparison of simple potential functions for simulating liquid water. J Chem Phys 79:926–935

Konrat R, Sterk H (1993) Cross-correlation effects in the transverse relaxation of multiple-quantum transitions of heternuclear spin systems. Chem Phys Lett 203:75–80

Korzhnev DM, Kloiber K, Kay LE (2004a) Multiple-quantum relaxation dispersion NMR spectroscopy probing millisecond time-scale dynamics in proteins: theory and application. J Am Chem Soc 126:7320–7329

Korzhnev DM, Kloiber K, Kanelis V, Tugarinov V, Kay LE (2004b) Probing slow dynamics in high molecular weight proteins by methyl-TROSY NMR spectroscopy: application to a 723-residue enzyme. J Am Chem Soc 126:3964–3973

Kroenke CD, Loria JP, Lee LK, Rance M, Palmer AG (1998) Longitudinal and transverse ^{1}H–^{15}N dipolar/^{15}N chemical shift anisotropy relaxation interference: unamiguous determination of rotational diffusion tensors and chemical exchange effects in biological macromolecules. J Am Chem Soc 120:7905–7915

Martyna GJ, Tobias DJ, Klein ML (1994) Constant pressure molecular dynamics algorithms. J Chem Phys 101:4177–4189

McKinney W (2010) Data structures for statistical computing in Python. In: van der Walt S, Millman J (eds) Proceedings of the 9th Python in science conference, pp 51–56

Millet O, Palmer AG (2000) The static magnetic field dependence of chemical exchange linebroadening defines the chemical shift time scale. J Am Chem Soc 122:2867–2877

Millman KJ, Aivazis M (2011) Python for scientists and engineers. IEEE Comput Sci Eng 13:9–12

Ming D, Brüschweiler R (2004) Prediction of methyl-side chain dynamics in proteins. J Biomol NMR 29:363–368

Norwood TJ, Tillett ML, Lian L-Y (1999) Influence of cross-correlation between the chemical shift anisotropies of pairs of nuclei on multiple-quantum relaxation rates in macromolecules. Chem Phys Lett 300:429–434

Nosé S (1984) A unified formulation of the constant temperature molecular dynamics methods. J Chem Phys 81:511–519

O'Connell NE, Grey MJ, Tang Y, Kosuri P, Miloushev VZ, Raleigh DP, Palmer AG (2009) Partially folded equilibrium intermediate of the villin headpiece HP67 defined by ^{13}C relaxation dispersion. J Biomol NMR 45:85–98

Oliphant TE (2007) Python for scientific computing. IEEE Comput Sci Eng 9:10–20

Palmer AG, Koss H (2019) Chemical exchange. Methods Enzymol 615:177–236

Pérez F, Granger BE, IPython (2007) A system for interactive scientific computing. IEEE Comput Sci Eng 9:21–29

Phan IQH, Boyd J, Campbell ID (1996) Dynamic studies of a fibronectin type I module pair at three frequencies: Anisotropic modelling and direct determination of conformational exchange. J Biomol NMR 8:369–378

Reddy JG, Pratihar S, Ban D, Frischkorn S, Becker S, Griesinger C, Lee D (2018) Simultaneous determination of fast and slow dynamics in molecules using extreme CPMG relaxation dispersion experiments. J Biomol NMR 70:1–9

Sastry GM, Adzhigirey M, Annabhimoju TD, R. & Sherman W (2013) Protein and ligand preparation: parameters, protocols, and influence on virtual screening enrichments. J Comput Aided Mol Des 27:221–234

Stafford KA, Robustelli P, Palmer AG (2013) Thermal adaptation of conformational dynamics in ribonuclease H. PLoS Comput Biol 9:e1003218

Stafford KA, Trbovic N, Butterwick JA, Abel R, Friesner RA, Palmer AG (2015) Conformational preferences underlying reduced activity of a thermophilic ribonuclease H. J Mol Biol 427:853–866

Toyama Y, Osawa M, Yokogawa M, Shimada I (2016) NMR method for characterizing microsecond-to-millisecond chemical exchanges utilizing differential multiple-quantum relaxation in high molecular weight proteins. J Am Chem Soc 138:2302–2311

Toyama Y, Kano H, Mase Y, Yokogawa M, Osawa M, Shimada I (2017) Dynamic regulation of GDP binding to G proteins revealed by magnetic field-dependent NMR relaxation analyses. Nat Commun 8:14523

Trott O, Siggers K, Rost B, Palmer AG (2008) Protein conformational flexibility prediction using machine learning. J Magn Reson 192:37–47

Tuckerman M, Berne BJ, Martyna GJ (1992) Reversible multiple time scale molecular dynamics. J Chem Phys 97:1990–2001

Tugarinov V, Kay LE (2006) Relaxation rates of degenerate ^{1}H transitions in methyl groups of poteins as reporters of side-chain dynamics. J Am Chem Soc 128:7299–7308

Tugarinov V, Kay LE (2007) Separating degenerate ^{1}H transitions in methyl group probes for single-quantum ^{1}H–CPMG relaxation dispersion NMR spectroscopy. J Am Chem Soc 129:9514–9521

Tugarinov V, Hwang PM, Ollerenshaw JE, Kay LE (2003) Cross-correlated relaxation enhanced ^{1}H–^{13}C NMR spectroscopy of methyl groups in very high molecular weight proteins and protein complexes. J Am Chem Soc 125:10420–10428

Tugarinov V, Sprangers R, Kay LE (2004) Line narrowing in methyl-TROSY using zero-quantum ^{1}H–^{13}C NMR spectroscopy. J Am Chem Soc 126:4921–4925

Tugarinov V, Kay LE, Ibraghimov I, Orekhov VY (2005) High-resolution four-dimensional ^{1}H–^{13}C NOE spectroscopy using methyl-TROSY, sparse data acquisition, and multidimensional decomposition. J Am Chem Soc 127:2767–2775

Tugarinov V, Ollerenshaw JE, Kay LE (2006) Dipolar dynamic frequency shifts in multiple-quantum spectra of methyl groups in proteins: correlation with side-chain motion. Magn Reson Chem 44:S122–S129

Tugarinov V, Sprangers R, Kay LE (2007) Probing side-chain dynamics in the proteasome by relaxation violated coherence transfer NMR spectroscopy. J Am Chem Soc 129:1743–1750

van der Walt S, Colbert SC, Varoquaux G (2011) The NumPy array: a structure for efficient numerical computation. IEEE Comput Sci Eng 13:22–30

Wang C, Palmer AG (2002) Differential multiple quantum relaxation caused by chemical exchange outside the fast exchange limit. J Biomol NMR 24:263–268

Wang C, Palmer AG (2003) Solution NMR methods for quantitative identification of chemical exchange in ^{15}N-labeled proteins. Magn Reson Chem 41:866–876

Williams CJ, Headd JJ, Moriarty NW, Prisant MG, Videau LL, Deis LN, Verma V, Keedy DA, Hintze BJ, Chen VB, Jain S, Lewis SM, Arendall WB, Snoeyink J, Adams PD, Lovell SC, Richardson JS, Richardson DC, MolProbity (2018) More and better reference data for improved all-atom structure validation. Protein Sci 27:293–315

York DM, Darden TA, Pedersen LG (1993) The effect of long-range electrostatic interactions in simulations of macromolecular crystals: a comparison of the Ewald and truncated list methods. J Chem Phys 99:8345–8348

Zhang F, Brüschweiler R (2002) Contact model for the prediction of NMR N–H order parameters in globular proteins. J Am Chem Soc 124:12654–12655